2021 43rd Annual International Conference of the
IEEE Engineering in Medicine & Biology Society (EMBC)
Oct 31 - Nov 4, 2021. Virtual Conference

Effective models of microwave antennae for ablation treatment planning

Zoi Tokoutsi[1], Marco Baragona[1], and Bruno Frackowiak[1]

***Abstract*— The level of detail of typical numerical models of microwave tumor ablations poses a challenge to the development of generic, model based treatment planning tools aiming at real time performance. The present contribution describes a flexible and accurate approximation of the microwave heat absorption that aims at mitigating these issues.**

***Clinical relevance*— Biophysical models are a promising tool towards standardization and improved planning of microwave thermal ablation procedures.**

I. INTRODUCTION

Thermal ablation cancer treatments are minimally invasive procedures that destroy the targeted tumor through thermal damage. Different modalities can be used, such as radiofrequency (RF), microwave (MW), cryoablation (cryo), see [1]. Ensuring full ablation of the tumor while sparing surrounding risk structures can be challenging, especially for larger tumors and tumors close to large blood vessels. Clinicians often rely on experience for their planning due to the discrepancy between observed ablations and manufacturer estimates (the latter being often based on ex-vivo animal or phantom tests).

Biophysical models show promising results as a tool to improve the prediction and planning of thermal ablations, [12], [3], [10]. These models may be particularly meaningful for MW, where measuring thermal damage during ablation is even more complex than for other modalities, for instance because of compatibility issues with MR thermometry (MRTI).

There are numerous approaches to modeling MW ablations treatments [9] and various attempts to validate these models in ex vivo [4], [6] and in vivo settings [8]. In silico approaches are extensively used in designing and optimizing ablation devices [13]. In addition, in recent years there have been attempts to employ MW models in clinical practice for estimating treatment outcomes and informing the guidance and planning of the treatment, e.g. [6].

In this work, we focus on the modeling of MW antennas in the context of treatment planning. The exact geometry and components of a MW antenna are in general unknown. They have, however, a significant effect on the electromagnetic field around it, and thus on the heating of tissue. This challenge introduces many uncertainties in the modeling of a specific MW antenna, and can hinder the development of generic treatment planning tools that are required to be not only patient, but also device specific.

Furthermore, even if the antenna specification is available, the components of a MW antenna are typically very small compared to the computational domain, and enforce restrictions to the element size of the mesh, which translate into relatively large computational times, becoming easily a bottleneck for real-time treatment planning.

We propose the use of simplified formulations of the heat source around the MW antenna, which can be constructed by combining shapes that represent the essential features present in an ablation device, e.g. the type of MW antenna and its size. Such general information is typically known, even if the details are not. The shapes are fitted to available data to reproduce the treatment outcome expected from the ablation device. Typical data include the ablation zones specified by the manufacturer, literature studies and measurements, and/or data measured in a dedicated experimental set up. In this paper, we describe a method for estimating the antenna specific heat source and illustrate the accuracy of such effective formulations with numerical results.

II. MICROWAVE ABLATION MODEL

The modeling of thermal tissue damage caused by a percutaneous microwave antenna typically involves the description of microwave propagation and absorption in tissue (defining the heat source Q_{MW}), a bio-heat equation (BHT) predicting the subsequent temperature increase and a thermal damage model translating the temperature field T(x,t) into an indicator of tissue damage probability. For more details we refer to [9]. In the next paragraphs, the choices made in the present work will be briefly illustrated.

A. Microwave Absorption in Tissue

The propagation of electric field E in lossy medium can be described by the Helmholtz equation. In frequency domain:

$$\nabla \times (\nabla \times E) - {k_0}^2 \left(\epsilon - i \frac{\sigma}{\omega \epsilon_0} \right) E = 0 \qquad (1)$$

The heat source Q_{MW} is then calculated as:

$$Q_{MW} = \frac{\sigma}{2} (E \cdot E) . \qquad (2)$$

Q_{MW} can be converted to specific absorption rate (SAR) by normalization with density ρ, i.e. $Q_{MW} = \rho \cdot SAR$.

The electrical properties σ and ϵ at $37°$ are taken equal to 1.9 (S/m) and 45 respectively, which are typical for human liver at 2.45 (GHz). A sigmoidal description is used for the dependence with temperature of electrical properties, as introduced in [4] with the corrections discussed in [5], that are particularly relevant at temperatures above $100°$. In the present work, the strong coupling with the BHT equation is relaxed by defining:

$$SAR'(x,T) = SAR(x,T_0) f(\epsilon(x,T), \sigma(x,T)) \qquad (3)$$

[1] All authors are with Philips Research, High Tech Campus 34, 5656AE Eindhoven, The Netherlands. zoi.tokoutsi@philips.com, marco.baragona@philips.com, bruno.frackowiak@philips.com

This approach allows to effectively split the SAR into a $SAR(x, T_0)$ term which has mainly to do with the characteristics of antenna construction and the operating frequency. And $f(T)$ which effectively models the change in SAR during ablation due to non-linear effects. The wave propagation equation can then be solved for the initial conditions only or $SAR(x, T_0)$ can be replaced altogether with an appropriate approximation, as will be further detailed later in the text.

The results obtained with the SAR computed by updating the E field at every time step have been compared for a limited set of exemplary cases ($75-100W$, $400-600s$ ablation time) to those obtained with SAR' using $f = p\frac{\sigma(x,T)}{\sigma(x,T_0)}$, with p a scaling factor related to power. The differences in the resulting ablated region and in maximum temperature at the end of ablation remained below 5% and 15% respectively, a result in line with similar comparisons reported in [6]. These error levels are typically below those introduced by other sources of uncertainty (e.g. needle positioning) and are thus considered acceptable for current practical applications.

B. Heat Transfer in Tissue

The BHT equation used in the present work is given by:

$$\rho C_{p_{eff}}(T)\partial_t T - \nabla(k(T)\nabla T) + C_{p_b} w_b(T)(T - T_b) = Q_{MW}(x, T) \quad (4)$$

The suffix b refers to blood. The perfusion rate $w_b(T)$ and the thermal conductivity $k(T)$ of liver are functions of temperature as described in [11], the values at 37° being respectively 5.0 $(kg/m^3 s)$ and 0.51 (W/mK). The heat capacity C_p is modified to take into account the latent heat of evaporation, which is particularly important for temperatures above 90°. Following [13], the effective heat capacity is defined as:

$$C_{p_{eff}} = C_p - \frac{\alpha}{\rho}\frac{\partial W}{\partial T}, \quad (5)$$

where $\alpha = 2260$ (kJ/kg) is the latent heat of water, W is the tissue water density (kg/m^3) and $\partial_T W$ is taken equal to the measured values reported in [13] with base water fraction of 70%. The density ρ and C_p are taken equal to 1080 (kg/m^3) and 3540 (J/kgK) respectively.

C. Thermal Damage

The thermal damage is estimated with a standard Arrhenius model, see for instance [9]:

$$\Omega(x, t) = \int_0^t A e^{-E_a/RT} dt \quad (6)$$

The activation energy E_a is set to $2.769e5$ (J/mol), the frequency factor A to $5.51e41$ (s^{-1}) [7]. R is the universal gas constant. The Arrhenius damage integral Ω can be used to estimate the probability of cell death $\theta(x, t) = 1 - e^{-\Omega}$.

III. EFFECTIVE MODELS FOR MW ANTENNAS

Based on the type of the MW antenna and the presence of gas or water cooling in the needle, each MW ablation device creates a distinct pattern of heat transferred to the tissue. The shape of its distribution can be effectively approximated by simple mathematical functions that capture its basic form. In the following, we create a simplified representation of the heat source generated by a MW antenna, which is able to reproduce with sufficient accuracy the increase of temperature and the ensuing ablation around a MW needle.

A. Benchmark Case

A detailed geometrical model is created of an insulated microwave antenna made of a proximal radiating section, essentially a monopole choke antenna, connected through the inner feed to a tapered distal radiating section. Furthermore, it is assumed that the radiating section is surrounded and actively cooled by a saline solution (which therefore acts also as a dielectric buffer). This construction is intended to be similar to state of the art MW devices such as the Emprint device [2]. The dimensions of the needle components have been roughly optimized to create ablations in the range of size and shape of those reported by real MW ablation systems, e.g. in [2]. The efficiency is optimized by minimizing the antenna's reflection coefficient. For the final construction, at the start of ablation, roughly 70% of the input power is delivered to the tissue. The computational solution of this model, see Fig. 1, enables us to generate ground truth reference data for benchmark and validation of the approximate method.

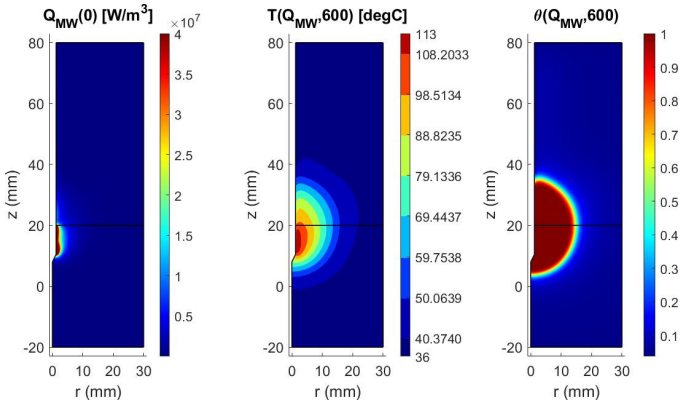

Fig. 1: A. Heat source at the beginning of ablation, B. Temperature distribution after 600 (s) of ablation, C. Thermal damage after 600 (s) of ablation.

B. Effective Model

Exploiting the radial symmetry of the modeled MW antenna, we can divide the heat source shape into a longitudinal and radial component. In particular at time $t = 0$ (s) the MW generated heat along and across the needle, is depicted in Fig. 2. The two peaks correspond to the location of the radiating sections of the antenna, and can be approximated by the sum of two Gaussian functions. The radial decay of heat can be described by the closed form of the SAR distribution as presented in [14].

In particular, we define the parameter $\mu = (a1, a2, c_1, c_2, z_{01}, z_{02}, n, r_0)$, where $a_1 \in [0.1, 10] \times 10^7$ (W/m^3), $a_2 \in [0.1, 1] \times a_1$, $c_1 \in [0.5, 2]$ (mm), $c_2 \in [2, 6]$ (mm), $z_{01} \in [11, 15]$ (mm) and $z_{02} \in [16, 21]$ (mm),

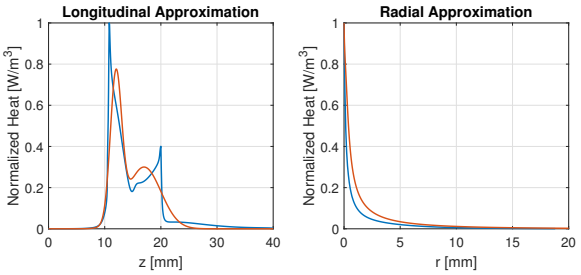

Fig. 2: Heat source along the surface of the ablation needle and across it. We plot in blue the ground truth Q_{MW} and in red an example of the effective heat source Q_{EF}. The z and r directions are indicated in Figure 1.

correspond respectively to the scaling, the variance and the center of the two Gaussian functions close to the peaks of the MW heat source. While $r_0 \in [0.1, 1.2]$ (mm) acts as an offset of the SAR from the geometric center of the catheter and $n \in [2, 3]$ corresponds to different approximations used for the analytic description of the SAR, for more details see [14] and references therein.

$$Q_z(z;\mu) = a_1 g(z; c_1, z_{01}) + a_2 g(z; c_2, z_{02}), \tag{7}$$

$$Q_r(r;\mu) = \frac{(2\alpha(r+r_0) + n - 2)\exp(-2\alpha(r+r_0))}{2(r+r_0)^n}, \tag{8}$$

where $g(z; c, z_0) = \exp\left(-(z-z_0)^2/(2c^2)\right)$ and $\alpha = 0.0413$ (mm^{-1}) in an attenuation constant. In addition, we can multiply the radial decay with a hyperbolic tangent function $h(r;\mu) = \tanh\left(5\left(r - r_0/2\right)\right)+1$, so that we reduce the total heat over the volume of the needle. This is relevant because in the following we optimize the parametrization of the effective heat source not only to match the ground truth, but also to match the heat that is dissipated into the tissue. The ensuing parametrized effective heat source is given by

$$Q_{EF}(r;\mu) = h(r;\mu) Q_r(r;\mu) Q_z(z;\mu) \tag{9}$$

C. Methods for Device Specific Parameter Identification

We identify appropriate values for the shapes parameter μ by solving a mathematical optimization problem. In particular, we minimize a cost function that comprises of an appropriate norm of the difference between a target field and the corresponding prediction of the model with the effective heat source. The target field can be any or a combination of the following: temperature distribution, thermal damage, ablation volume, point temperature measurements and others. In the following we define different possible formulations for the cost function and present the results of the solutions to the corresponding minimization problems.

1) Optimization with respect to target temperature: In order to identify the model parameters for Q_{EF} so that the temperature distribution between the ground truth and the effective model match, we minimize the cost function

$$f_I(\mu) = \omega_1 f_T^{KN}(\mu) + \omega_2 f_{\bar{Q}}(\mu), \tag{10}$$

where $f_T^{KN}(\mu) = \sum_{k=1}^{K}\sum_{i=1}^{N}\left((T^k_{MW,i} - T^k_{EF,i})/T^k_{MW,i}\right)^2$ is the squared mean relative difference between effective and target temperature with $T^k_{\bullet,i}$, $i = 1,\dots,N$, $k = 1,\dots,K$ being temperature data at N spatial locations at K time points computed with the MW (MW) or the effective (EF) heat source, $f_{\bar{Q}}(\mu) = \left((\bar{Q}_{MW} - \bar{Q}_{EF})/\bar{Q}_{MW}\right)^2$ is the squared relative difference between the effective and target total heat $\bar{Q}$ at the beginning of ablation, and ω_1, ω_2 are user defined weights.

2) Optimization with respect to target thermal damage: Analogous to the temperature formulation we define a cost function that ensures that μ is such that the thermal damage of the approximate model matches the ground truth, i.e.

$$f_{II}(\mu) = \omega_1 f_\theta^{KN}(\mu) + \omega_2 f_{\bar{Q}}(\mu), \tag{11}$$

where $f_\theta^{KN}(\mu) = \sum_{k=1}^{K}\sum_{i=1}^{N}\left((\theta^k_{MW,i} - \theta^k_{EF,i})\right)^2$ corresponds to the difference between effective and target thermal damage and $f_{\bar{Q}}$, ω_1 and ω_2 are as in (10).

3) Optimization with respect to target thermal damage and point temperature measurements: In the case where point temperature measurements are available, e.g. via thermocouple measurements close to the ablation needle, we can extend cost function (11) as follows:

$$f_{III}(\mu) = \omega_1 f_T^{KN}(\mu) + \omega_2 f_\theta^{LM}(\mu) + \omega_3 f_{\bar{Q}}(\mu), \tag{12}$$

where f_T^{KN} is as in (10), f_θ^{LM} is analogous to (11), and $N << M$ and $L << K$ because we have only a few temperature measurements at a high temporal resolution, but know the distribution of thermal damage only at a few time points. Again ω_i, $i = 1, 2, 3$ are user defined weights.

IV. NUMERICAL RESULTS

Solutions to both the MW and the effective models are computed using the finite element method (FEM) in a hybrid environment: COMSOL 5.5 coupled with MATLAB R2020b. The optimization problems for determining the model parameter μ of the effective heat source are solved in MATLAB using the therein available Bayesian optimization method. Bayesian optimization is an appropriate choice for global optimization problems, where the cost function is expensive to evaluate.

We compute solutions to optimization problems with the following five variations of the above defined cost functions: (Opt Ia) optimize $f_I(\mu)$ with $\omega_1 = \omega_2 = 1$, (Opt Ib) optimize $f_I(\mu)$ with $\omega_1 = 1/(NK)$ and $\omega_2 = 1$, (Opt IIa) optimize $f_{II}(\mu)$ with $\omega_1 = \omega_2 = 1$, (Opt IIb) optimize $f_{II}(\mu)$ with $\omega_1 = 1/(NK)$ and $\omega_2 = 1$, and (Opt III) optimize $f_{III}(\mu)$ with $\omega_1 = \omega_3 = 1$ and $\omega_2 = 10/(LM)$. The weights are chosen so that all terms in the cost function are of the same order of magnitude. Different weight combinations can result in different optimal solutions. Although optimizing the weights would be possible, it would be very computationally expensive and is omitted from this study.

We expect that by down-weighting f_T^{KN} or f_θ^{KN} we enhance the importance of the total heat in the effective model matching that of the MW model. Whereas in Opt III by down-weighting f_θ^{LM} we achieve a balanced cost function where all three terms have similar magnitudes. This

is reflected in the results presented in Table I, where we present different errors between the effective model and the ground truth. In particular, the root mean squared error (RMSE) E_F for a field $F = (F_i^k)_{i=1,\dots,N}^{k=1,\dots,K}$, computed with the MW model F_{MW} and the effective model F_{EF} is given by $E_F = (\sum_{k=1}^{K} \sum_{i=1}^{N} (F_{MW,i}^k - F_{EF,i}^k)^2/(NK))^{1/2}$, where N is the number of points in the spatial and K the number of time steps in the temporal discretization of the problem. The RMSE for the ablation volume in time is given by $E_V = (\sum_{k=1}^{K} (V_{MW}^k - V_{EF}^k)^2/K)^{1/2}$. Finally, the percent error $\mathcal{E}_\phi$ for a scalar ϕ is given by $\mathcal{E}_\phi = 100\% \times |\phi_{MW} - \phi_{EF}|/\phi_{MW}$ and it is used to compute the error in the total heat and the end ablation volume.

TABLE I: Various errors between optimized effective model and ground truth for the different cost functions.

Error	Opt Ia	Opt Ib	Opt IIa	Opt IIb	Opt III
E_T $(^\circ C)$	1.3350	1.8649	1.5022	1.4242	1.5053
E_θ	0.1868	0.3146	0.1910	0.2007	0.2311
E_V (cm^3)	0.2518	2.5479	0.5330	0.5591	0.5237
$\mathcal{E}_{V_{end}}$	3.3%	30.1%	0.07%	7.9%	0.2%
$\mathcal{E}_{Q_{tot}}$	20.2%	0.8%	13.9%	1.6%	4.5%

All solutions, except for Opt Ib, can reproduce the ground truth ablation volume to a satisfactory level, see Fig. 3. The result of Opt Ia has the smallest RMSE for the temperature and consequently also the thermal damage, but a larger percent error for the total heat. On the other hand, Opt Ib matches well the total heat, with less than 1% difference from the ground truth, at the expense of the temperature and thermal damage. The miss-match in temperature results in a significant enlargement of the ablation volume. This is reflected in both the yellow lines in Figure 3 and the corresponding E_V and $\mathcal{E}_{V_{end}}$ in Table I, with the end ablation volume being 30% larger than the ground truth. We expect however, that further adjustments to the weights of Opt Ib can improve the result. This is strengthened by the outcome of Opt IIb and III, where the terms in the cost function are more evenly balanced and a good agreement in temperature, ablation and thermal energy is achieved.

In the above examples we consider different possibilities for available ground truth data. Opt I examines the case where temperature measurements at every point of the spatial discretization and at every minute of simulation time are available. In Opt II we assume that the thermal damage is known at every point of the spatial discretization and at every minute of simulation time. In Opt III we assume to have the distribution of θ only at 5 and 10 minutes, while we have temperature measurements every 2 seconds on five locations, two on the probe and three at 4, 8 and 12 (mm) away from the probe. In real practice, such target data could be derived from the MW device manufacturer specifications, previous ablations and thermocouple measurements. The results presented above show the consistency of the optimization and allow us to adapt the method depending on the ground truth available in real setting. Hence, we are confident that this approach allows to incorporate more easily new clinical data or device

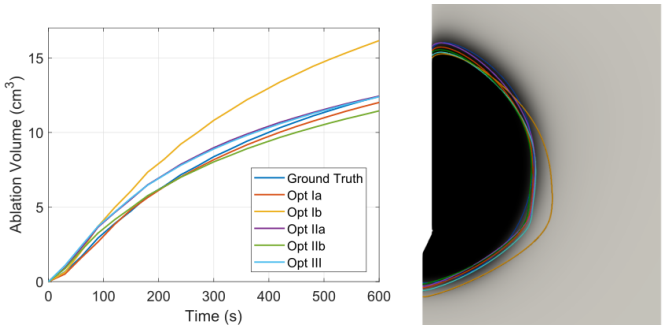

Fig. 3: Ground truth versus optimized effective model ablations. Left: volume growth in time. Right: isolines of the ablation after 10 minutes over the distribution of θ_{MW}. The similarity of the different approximations gives us confidence that this approach can be effective for different scenarios depending on data availability.

knowledge, when available, thereby continuously improving the effective model and the accuracy of its predictions. The applicability of the full model and the effective description in clinical setting is currently being tested in clinical studies.

References

[1] K. F. Chu and D. E. Dupuy. Thermal ablation of tumours: biological mechanisms and advances in therapy. *Nature reviews. Cancer*, 14 3:199–208, 2014.

[2] F. De Cobelli, P. Marra, F. Ratti et al. Microwave ablation of liver malignancies: comparison of effects and early outcomes of percutaneous and intraoperative approaches with different liver conditions. *Med Oncol*, 34(49), 2017.

[3] E. Golkar, P. P. Rao, L. Joskowicz et al. GPU-based 3D iceball modeling for fast cryoablation simulation and planning. *Int J CARS*, 14:1577–1588, 2019.

[4] Z. Ji, C.L. Brace. Expanded modeling of temperature-dependent dielectric properties for microwave thermal ablation. *Phys Med Biol.*, 21;56(16):5249-64, 2011.

[5] V. Lopresto, R. Pinto, M. Cavagnaro. Experimental characterisation of the thermal lesion induced by microwave ablation. *Int J Hyperthermia*, 30(2):110–8, 2014.

[6] V. Lopresto, R. Pinto, L. Farina, and M. Cavagnaro. Treatment planning in microwave thermal ablation: clinical gaps and recent research advances. *International Journal of Hyperthermia*, 33(1):83–100, 2017.

[7] E. G. Moros. Physics of Thermal Therapy Fundamentals and clinical applications, 2013.

[8] R. Ortega-Palacios et al. Feasibility of using a novel 2.45 GHz double short distance slot coaxial antenna for minimally invasive cancer breast microwave ablation therapy: Computational model, phantom, and *In Vivo* swine experimentation. *Journal of Healthcare Engineering*, 2018.

[9] P. Prakash. Theoretical modeling for hepatic microwave ablation. *The Open Biomedical Engineering Journal*, 4:27 – 38, 2010.

[10] C. Rieder, T. Kroeger, C. Schumann, and H. K. Hahn. GPU-based real-time approximation of the ablation zone for radiofrequency ablation. *IEEE Transactions on Visualization and Computer Graphics*, 17(12):1812–1821, Dec 2011.

[11] N. Tsafnat et al. Modelling heating of liver tumours with heterogeneous magnetic microsphere deposition. *Phys. Med. Biol.*, 50:2937, 2005.

[12] P. Voglreiter, et al. RFA guardian: Comprehensive simulation of radiofrequency ablation treatment of liver tumors. *Scientific Reports*, 8(1), 2018.

[13] D. Yang. Measurements, antenna design and advanced computer modeling for microwave tissue ablation, 2005.

[14] L. Zhu, L. X. Xu, N. Chencinski. Quantification of the 3-D electromagnetic power absorption rate in tissue during transurethral prostatic microwave thermotherapy using heat transfer model. *IEEE Trans Biomed Eng.*, 45(9):1163-72, 1998.